J. Eng. Technol. Sci., Vol. 54, No. 6, 2022, 220603

The Combined Use of Terrestrial Laser Scanner and Handheld 3D Scanner for 3D Modeling of Piping Instrumentation at Oil and Gas Company

Irwan Gumilar[1,*], Farhan Farohi[2], Made Munarda[3], Brian Bramanto[1] & Gusti Ayu Jessy Kartini[2,4]

[1]Geodesy Research Group, Faculty of Earth Sciences and Technology, Institut Teknologi Bandung, Jalan Ganesa 10, Bandung 40132, Indonesia
[2]Geodesy and Geomatics Engineering, Faculty of Earth Sciences and Technology, Institut Teknologi Bandung, Jalan Ganesa 10, Bandung 40132, Indonesia
[3]Tri Panji Puring Ltd, Buncit Business Center (BBC) Blok B-6 Jalan Buncit Raya No. 24, Jakarta 12760, Indonesia
[4] Geodetics Engineering, Faculty of Civil Engineering and Planning, Institut Teknologi Nasional Bandung, Jalan PHH. Mustofa No. 23, Bandung 40124, Indonesia
*E-mail: igumilar@itb.ac.id

Highlights:

- The combined use of a terrestrial laser scanner and a handheld 3D scanner enables the user to retrieve complete point clouds of complex objects.
- The accuracy of the generated 3D models is up to a few millimeters.
- The resulting 3D models can be used for labeling piping instrumentation.

Abstract. Three-dimensional (3D) models are indispensable in managing and operating piping instrumentation activities in oil and gas companies. A 3D model provides more interactive and representative information about the actual object. Technologies that can be used to generate 3D piping instrumentation maps are the terrestrial laser scanner (TLS) and the handheld 3D scanner (HS). This study aimed to create a 3D model of piping instrumentation based on a combination of the TLS and HS methods. The results showed that an accurate 3D piping instrumentation model could be generated by combining these two methods. Merging the two data sets was carried out through a cloud-to-cloud registration process based on the object's geometry by considering the selection of reference data, the similarity of the scale factor, the unit of measure, and the overlap of the two data. The registration error generated in combining these two methods was less than 3 mm. The geometric validation of the model's dimensions using reference data and in-situ measurements had a largest absolute difference of 3.4 mm and an average absolute deviation of 1.6 mm.

Keywords: *3D model; accuracy; handheld 3D scanner; piping instrumentation; point cloud; terrestrial laser scanner.*

Received April 7th, 2022, 1st Revision August 8th, 2022, 2nd Revision September 9th, 2022, Accepted for publication September 22nd, 2022.

DOI: 10.5614/j.eng.technol.sci.2022.54.6.3

1 Introduction

Nowadays, 3-dimensional (3D) high-resolution mapping is widely used for various applications, e.g., terrestrial mapping [1], heritage conservation [2], and indoor mapping [3]. 3D mapping also plays an essential role in the oil and gas sector other than for producing terrestrial maps. For example, one can produce a 3D model of an object of interest such as piping instrumentation for management, operation, maintenance, and repairs, for present or future purposes.

Recent technologies that can be used to produce a 3D piping instrumentation model are the terrestrial laser scanner (TLS) and the handheld 3D scanner (HS). Both are laser-based technologies capable of recording a large number of points with an accuracy of up to several millimeters in a relatively short manner [4]. The collected points from these bespoke technologies are also called point clouds. The point clouds generated by TLS and HS represent the shape of the surface of the scanned object with a certain point density, depending on the specification of the survey and instrument capability.

TLS can be applied in many fields, for example, for mining [5], architecture [6], civil engineering [7], crime investigation [8], and geological [9] purposes. Several studies related to the use of TLS for piping instruments have been carried out in several countries. Wakisaka, *et al.* [10] proposes a novel method to efficiently generate 3D models in the heating, ventilating, and air-conditioning (HVAC) industry using TLS. Gumilar, *et al.* [11] used TLS for 3D modeling and assessment of tank conditions in an oil and gas company. Allard and Mony [12] examined pipeline corrosion using a laser scanner. Additionally, TLS can also be used to measure the level of corrosion of steel elements [13]. Walach and Kaczmarczyk [14] further combined point clouds derived from TLS with the finite element method (FEM) to determine the actual technical condition of several essential steel elements in a historic building. A normal-based region growing algorithm was applied to automatically identify a piping system from TLS data by Kawashiwa, *et al.* [15]. The detection was not only limited to simple pipe shapes, e.g., straight-shaped pipes, but was also able to recognize more complicated shapes, such as elbows and junction-shaped pipes.

On the other hand, measurements using HS are widely used in reverse engineering in the automotive [16], medical, and aerospace sectors, for example. In addition, HS has also been used in the craniometry sector [17]. Currently, the Apple iPhone 12 Pro can serve as an HS device. Luetzenburg, *et al.* [18] evaluated the Apple iPhone 12 Pro for geosciences applications. The LiDAR sensors implemented in the Apple iPhone 12 Pro can generate accurate high-resolution models of small objects with a side length of larger than 10 cm, with an absolute accuracy of approximately 1 cm.

Considering the application for complex object modeling, e.g., 3D piping modeling in the oil and gas industries, the use of TLS-only suffers practical difficulties in obtaining complete point clouds covering the whole object of interest. For example, in some cases the TLS cannot be positioned properly due to limited available space. The flexibility of HS is expected to address this issue in order to obtain optimal point clouds for modeling purposes.

The combination of HS and TLS has not been widely discussed, especially not for piping instrumentation modeling. Some modeling applications are based on TLS-only observations. In addition, most of the studies compared HS and TLS for accuracy analysis [19]. Therefore, this study aimed to combine TLS and HS measurements to better represent the object of interest that are beneficial for 3D modeling applications. One of the keys to successful 3D modeling is the density of the point clouds to mimic the original shape. This study focused on the application of TLS and HS to model complex piping instrumentations at an Indonesian oil and gas company from point cloud data. Finally, the point clouds were also evaluated to assess the accuracy of the data.

2 Fundamental Aspects and Research Methodology

In this section, the laser scanner system, including the concepts of time-based measurement and the point cloud, are briefly discussed. Further, an overview of how a handheld 3D scanner works is given. Finally, the research methodology applied in this study is addressed.

2.1 Overview of Laser Scanner System

Most laser scanner systems use the so-called pulse-based or time-of-flight principle to measure the range between the sensor and the object. The long dynamic range of the time-of-flight principle makes it more useful for various applications, as it can be used for close and long-range observation [20,21]. The pulse-based principle's main property is the propagation of light waves in a certain medium from a source to a reflective target. Eventually, the target reflects the light waves back to the source; the time needed for the light waves to make a round trip is estimated. Mathematically, the range obtained using the pulse-based principle can be written as follows:

$$R = (vt)/2 \tag{1}$$

where R is the distance between the sensor and the object; v is the speed of the electromagnetic wave; and t is the wave propagation time.

The results obtained from laser scanner measurements are point clouds with three-dimensional coordinates. A point cloud is a collection of points with a

certain point density, which can be used to form a surface or as three-dimensional modeling material [4]. Each point has 3D coordinate values (*x, y, z*) in a local system, and an intensity value (*i*). The coordinates can be calculated using the conventional polar and tacheometry methods from range and angle data obtained by measurement. The intensity value is influenced by the laser power, the nature of the object affecting the reflection, atmospheric transmission, and the distance from the sensor to the target [22].

2.2 Overview of Handheld 3D Scanner

One of the methods implemented in the HS system to obtain point clouds to represent an object of interest is the so-called structured light scanner. It is considered a non-destructive testing method that uses a video projector to continuously transmit multiple light patterns to the investigated object, which are then captured by a video camera or a photographic camera [23]. The benefit of the structured light scanner method is the fast scanning performance compared to other methods such as laser-based scanning.

There are at least three aspects required to estimate the 3D coordinates of each point. They are: (i) capturing the distorted light patterns due to the object of interest by using the attached camera, (ii) knowing the angles between the projection and observation systems such as the camera, and (iii) understanding the length of the optical basis connecting the nodal points or projection centers of both systems. Having all of these aspects known, a triangulation algorithm and stereoscopic parallax can be implemented to estimate the spatial position of the object. Additionally, if the HS is equipped with an RGB camera, the user can generate textured prints [24].

2.3 Research Methodology

The research methodology in 3D modeling in this study involved planning and preparation, reconnaissance survey, data acquisition, registration process, filtering, and 3D modeling. Data acquisition using TLS was done from several data sets. These sets of scans have their own orientation, which requires further procedures to create a complete point cloud. This procedure is called registration. The orientation of at least one scan set has to be fixed. The other scan set orientations can be adjusted to fit this fixed orientation with several techniques, such as point-to-point coordinate transformation or manual adjustment, by giving translation and rotation parameters. The georeferencing process can be implemented on the point cloud data when we need true coordinates on the produced map. Some of the scanned objects, such as trees, marsh and any vegetation cover, may not be used or visualized in the produced map. Therefore,

we need to apply filtering procedures. Filtering can be done manually or using an automatic algorithm.

The registration method used in this study was the cloud-to-cloud method. The registration stage is divided into three steps. The first step is registration of the TLS data, the second step is registration of the HS data, and the third step is registration of the combination of the TLS and the HS data. Georeferencing was done by using three points that have been measured using the Global Navigation Satellite System (GNSS). GNSS points were measured for 30 minutes relative to the oil and gas company's nearest control point. 3D modeling of pipeline instrumentation was carried out based on the combination of the TLS and the HS point cloud data. The 3D modeling was done by making several basic shapes whose sizes and geometries were arranged so that they matched the geometry of the object's point cloud.

Planning the position of the TLS station was carried out based on photos from photogrammetric UAV (Unmanned Aerial Vehicle) measurements, supported by checking conditions directly in the field during the preliminary survey. The location of TLS standpoints considers the appearance of certain scanning objects between adjacent standpoints. This is because this study chose the cloud-to-cloud registration method as the registration method, which requires well overlapping point clouds. The study area and the distribution of the TLS standpoints can be seen in Figure 1. In this study, the location for using HS was based on objects that were not covered by the TLS scanning. The area covered by the HS measurements is also depicted in Figure 1.

The instruments used in this research were a Topcon GLS 2000 TLS and a Stonex F6 HS. The claimed accuracy of the Topcon GLS 200 is in millimeter levels. It is considered a short-to medium-range scanner, which allows the user to obtain relatively dense point clouds when used to scan from a relatively short distance. In this study, the distance between TLS standpoints was set to not longer than 10 meters. Considering this setup, the point interval of an object at 10 meters is about 6 to 10 mm. The accuracy and the corresponding point density were adequate for our purposes. The Stonex F6 has been used widely for the documentation of small artifacts due to its accuracy and high point density [24]. The accuracy ranges from 90 μm at 0.25 meters to 0.5 mm at a distance of 1 meter. The resolution reaches 0.4 mm at 0.25 meters. To ensure a high accuracy and density of the point cloud, when using the Stonex F6, the distance between the sensor and the object was set to not longer than 1 meter. The accuracy and point density of these instruments allow the user to merge the resulting point clouds without significantly degrading the accuracy. In addition, the Topcon GR5 GNSS was also used for the georeferencing process. The main specifications and measurement setups of the TLS and HS tools can be seen in Table 1.

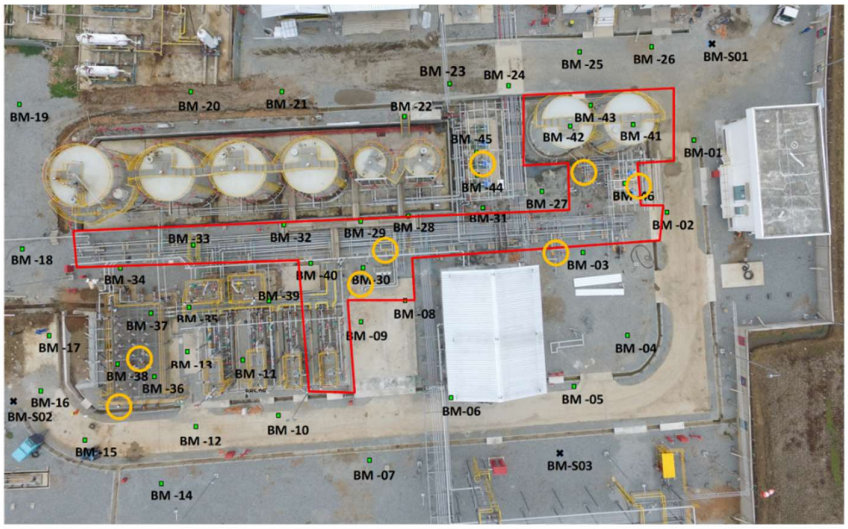

Figure 1 Bird's eye view of our study area. The distribution of the TLS standpoints and reference points used for the georeferencing process is shown by the green squares and black crosses, respectively. Yellow circles represent the areas that were covered by the HS. The red polygon indicates the object of interest.

Measurements were made by considering several aspects, such as available backup power and battery, scan range, station position, scanning resolution used, weather, as well as worker activity, and field obstructions. TLS and HS measurements were carried out for three days, including GNSS measurements. Several measurement documentations can be seen in Figure 2.

(a) (b) (c)

Figure 2 Documentation of (a) TLS, (b) HS, and (c) GNSS measurements.

Table 1 Key specifications and measurement setups of TLS and HS used in this study.

Parameter	TLS Topcon GLS2000	HS Stonex F6
Scan range	Up to 350 m	4.5-0.5 m
Data acquisition speed	Up to 120,000 points/second	640,000 points/second
Accuracy	3.5 mm (1-150m)	90 µm at 0.25 meters and 0.5 mm at 1 meter
Maximum distance between sensor and object	10 meters	1 meter
Scan quality (resolution)	High (6-10 mm at 10 meters)	- (0.4 mm at 0.25 meters)

3 Results and Discussion

3.1 Georeferencing

In this study, the georeferenced step is essential because the final result of this study is a 3D map georeferenced to the global coordinate system (World Geodetic System 1984/WGS84) using the UTM zone 48S projection coordinate system. Georeferencing is performed on the TLS backsighting scanned data. There were three positions for backsighting, i.e., BM-S01 to BM-S02, BM-S02 to BM-S03, and BM-S03 to BM-S02. These points were referenced to a nearby high-order reference point with a distance of less than 5 km by using a static differential positioning with a radial (single baseline) scheme. The distribution of BM-S01, BM-S02, and BM-S03 can be seen in Figure 1. The accurate positions for these points were obtained from the GNSS measurement results. The measurements were carried out using a Topcon GR-5 GNSS receiver with a static radial method. The results obtained for the coordinates of the control points can be seen in Table 2.

Table 2 Coordinates of control points (in meters).

Point	Easting	Northing	Height
BM-S01	760421.0599 ± 0.0001	9305183.8362 ± 0.0002	30.9454 ± 0.0004
BM-S02	760370.2204 ± 0.0001	9305206.6883 ± 0.0002	31.3471 ± 0.0003
BM-S03	760381.2194 ± 0.0002	9305272.4721 ± 0.0002	31.4145 ± 0.0003

The TLS georeferencing process was not carried out directly during the measurement but was carried out after the measurement. This was done because when the measurement was carried out, the coordinates of the control point were not yet known. In a direct georeferencing process, it is necessary to enter the coordinates of the standpoint, the target standpoint, the instrument height, and the target height.

3.2 Registration and Filtering Process on TLS Measurements

TLS data registration was carried out manually using the cloud-to-cloud method in two steps: the single registration step between scans, and global registration. Single registration between scans is a chain registration of scans from each nearest station, starting from the scan of the georeferenced station. Global registration is carried out to unite each previous single registration so that the quantitative value of the registration accuracy of each station to the other stations can be identified. In this study, the cloud-to-cloud registration method was chosen so that the appearance of the scanning objects was easily identifiable, such as the surface of the building and the corners of the structure.

The root mean square error (RMSE) threshold value for registration was set to 0.010 m with the aim of avoiding outliers that may occur during registration. The RMSE of registration verification results reached 0.003 meters, indicating good registration accuracy. In terms of internal accuracy, the RMSE value indicated that the registration results were good. The registered point clouds can be seen in Figure 3. Filtering was done manually by interpreting the point clouds visually before and after the registration process. The purpose of filtering is to remove noise and unwanted objects. Removing the amount of noise and unwanted objects can improve the quality of the registration RMSE and make it easier to identify objects during 3D modeling. The unwanted objects removed in the measurement area included human, heavy equipment, plants, piles of garbage and materials. The filtering process cannot be done automatically, as the method that is commonly introduced in the software is not fit for removing noise of complex objects, except for topography.

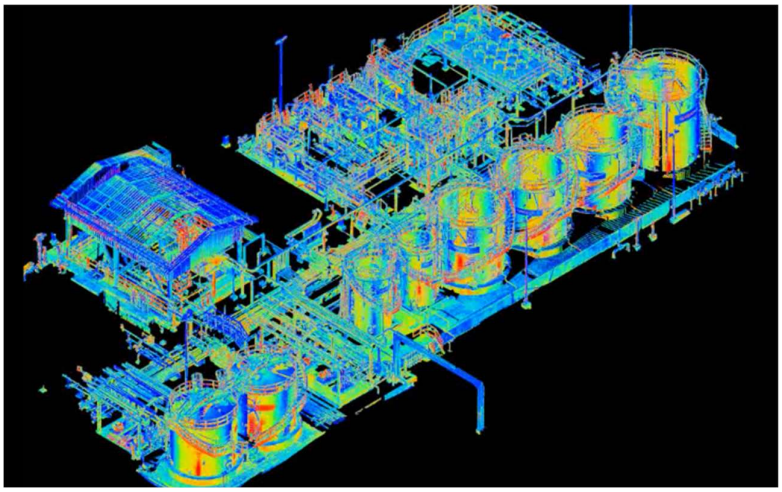

Figure 3 Registration result of TLS point clouds.

3.3 Registration and Filtering Process on HS Measurements

Data processing for HS measurements begins with the removal of segments with a small number of frames, followed by high-quality (HQ) registration between scan frames, editing and merging, global registration, noise removal, and scan data conversion. However, it should be noted that this process does not always produce good results, for example when scanning shaded objects. This is due to the software's inability to detect overlapping frames. When this is the case, the registration should be performed manually by adjusting the translation and rotation parameters. Finally, global registration is applied to the data. This combines all individual frames into a single group with the same coordinate reference system. Two algorithms, Moving Least Square (MLS) and Statistical Outlier Removal (SOR), were applied to the data to remove the remaining noise from these results. Some of the appearances of objects from the registration and filtering of the HS data can be seen in Figure 4.

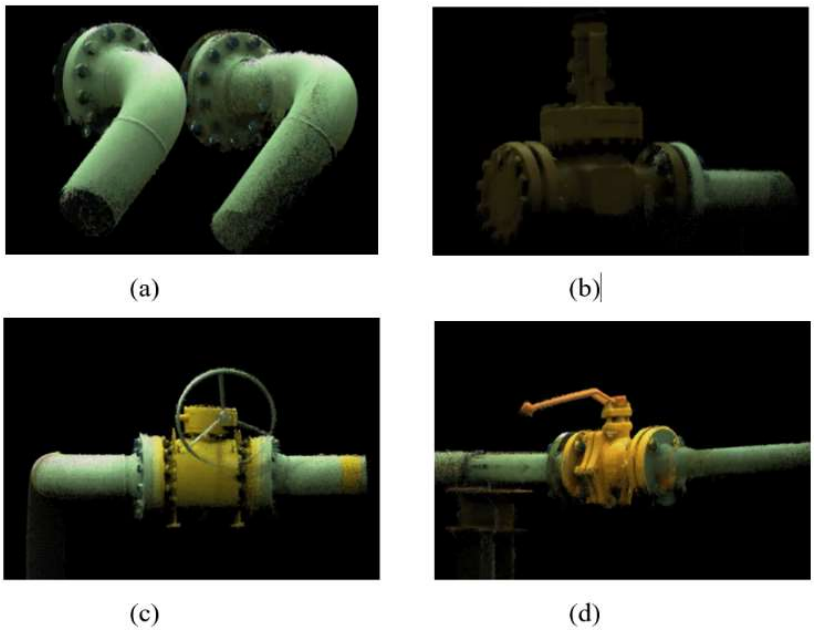

Figure 4 Registration result of handheld 3D scanner on flange and blind flange (a), gate valve (b), ball valve (c), and butterfly valve (d).

3.4 Combination of TLS and HS data

Merging TLS with HS data aims to obtain scanning data for all objects. This is because some objects cannot be scanned by TLS during the measurement due to

the object being covered by other objects. The obstruction of objects by other objects during TLS scanning is caused by improper placement of the instrument or because the area around the object is too narrow for the TLS to be positioned. As a result, the obtained point cloud will be incomplete so it cannot be used as a reference in 3D modeling.

To combine the TLS and HS point clouds, the transformation parameters (translation and rotation parameters) were first determined by manually selecting the identified common points from both measurements. This method is similar to the methodology proposed by Sadikin, *et al.* [25] and Suwardhi, *et al.* [26] to combine measurements from different references. The parameters were then applied to the HS point clouds, making it possible to obtain complete point clouds from the combination of the TLS and HS measurements. Since the coordinate reference system of the TLS point clouds has been defined in the georeferencing process, the transformed HS point clouds also refer to the same coordinate system as the TLS point clouds. The combination of the two data sets resulted in RMSE values between 0.002 and 0.003 m. There are several points that must be considered during the combination process:

1. TLS data is fixed and used as the reference

TLS data was chosen as the registration reference because this study aimed to produce 3D maps that are georeferenced to global coordinates. For this reason, the TLS data used was georeferenced TLS data.

2. The handheld 3D scanner data must have the same scale factor and unit of measure as the TLS data. Dissimilarity of the scale factor and the unit of measure between the two data sets can make it impossible to combine them. Setting the scale factor and unit of measure on the TLS and HS data was carried out during the initial acquisition and processing of the data. It is very important to always ensure the accuracy of the scale factor and unit of measure used during the process.

3. Parts of the object must overlap between the TLS with the HS data

The benefit of having object parts that overlap between the TLS and HS data is as reference for unification when registration is carried out. Without overlapping parts, the two data cannot be registered. Therefore, during scanning using an HS, it is better if the scanning is exaggerated by scanning several parts of the main object. On the other hand, it must also be ensured that the section is visible and scannable from the nearby TLS stations. An example of the result of the merged data can be seen in Figure 5.

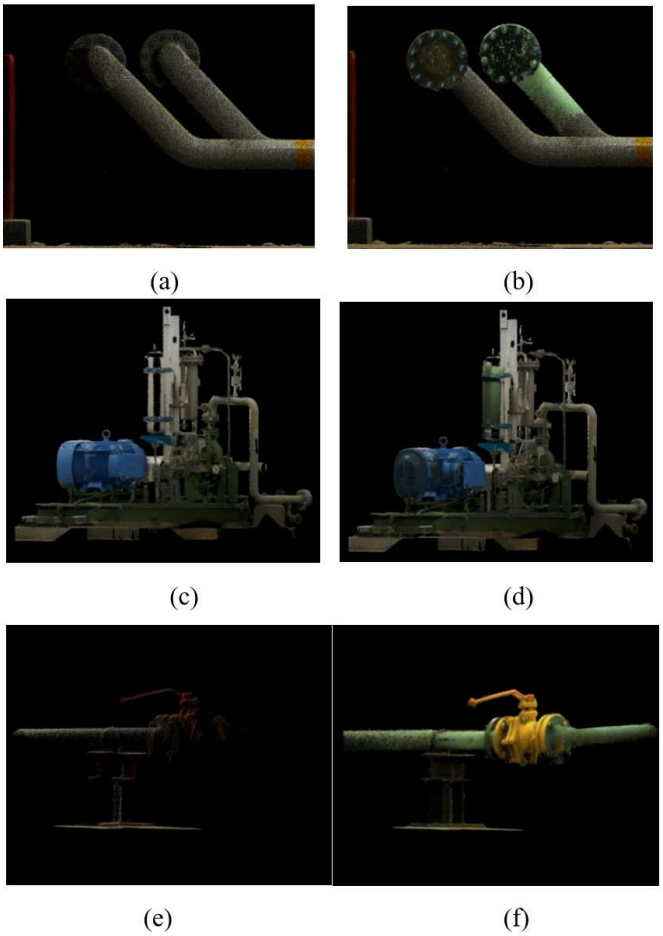

Figure 5 TLS-only point clouds (a, c, e) and combination between TLS and HLS point clouds (b, d, f).

3.5 3D Modeling

3D modeling was done using the Cyclone software. Before modeling, after all the data has gone through the process of georeferencing, registration, filtering, and merging, the HS and TLS data first need to be unified. Basically, modeling is done in three main stages, e.g., selecting a sample of the object to be modeled, cleaning the sample, and forming the elements of the 3D model. The object modeling is adjusted according to the ASME (American Society of Mechanical Engineers) and ANSI (American National Standards Institute) measurement standards. An illustration of the modeling result can be seen in Figure 6.

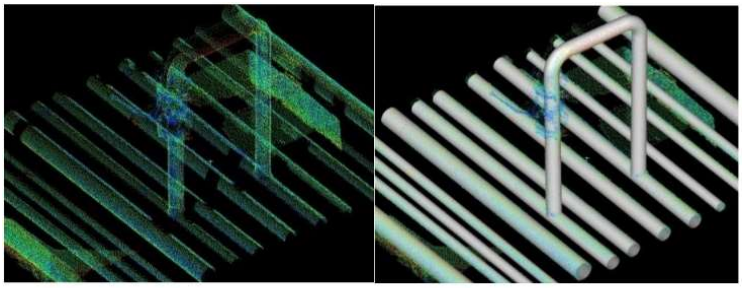

(a) (b)

Figure 6 Point cloud sample (a) and modeling result (b).

The 3D models created can be grouped into four categories, namely, equipment, pipes, structures, and surfaces. The equipment category includes tanks and separators equipped with connecting nozzles. The pipe category includes pipe cylinders, valves, and flanges. The structural category includes pipe supports and ladders. The formation of a 3D model of the pipe instrumentation was carried out based on the cloud point scan and size standards. This was also done for the other object categories. After obtaining the shape of the pipe, the pipe was separated into groups based on its function to make it easier to identify the path of the process. The following is a detailed explanation of the 3D modeling of each object.

3.5.1 Pipe Cylinder

Pipe cylinder modeling is done automatically. The model is made according to the appearance of the point cloud by adjusting the pipe size standards according to the provisions of ASME (American Society of Mechanical Engineers) and ANSI (American National Standards Institute). An example of a pipe cylinder model after being adjusted to the standard size is shown in Figure 7. The standard adjustment of the pipe size was carried out after the pipe cylinder plane was obtained from the results of point cloud reconstruction. During the modeling, there were deviations in the size of the reconstructed pipe, for example, deviations in a 6-inch diameter pipe with a diameter of 5.5 inches or 4.5 inches at the time of the pipe cylinder reconstruction. These deviations can occur due to the inaccuracy of selecting point cloud samples as reference for reconstructing the model. Due to the absence of a piping and instrumentation diagram (P&ID), these deviations were manually identified according to the usual pipe sizes based on expert modeling experience. In the modeling that was carried out, the largest deviation that occurred was no more than 0.5 inches and it only occurred in a few objects.

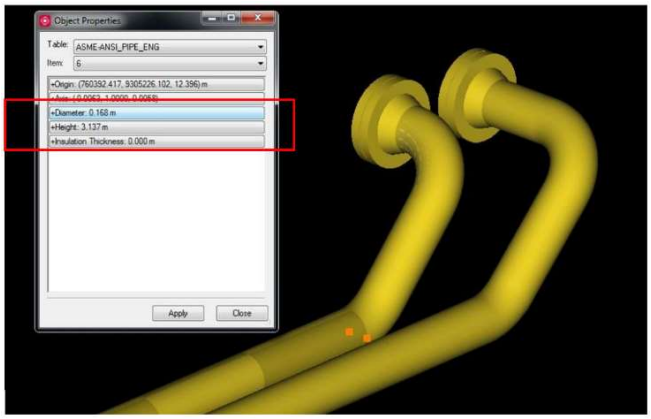

Figure 7 Sample pipe size according to the standard.

3.5.2 Elbow

The standard bend radius of the pipe elbow was determined based on the point cloud. Due to the absence of P&ID, the bend radius size was obtained by experimenting with each available size until an elbow had the exact geometry that coincided with the point cloud. An example of elbow modeling can be seen in Figure 8.

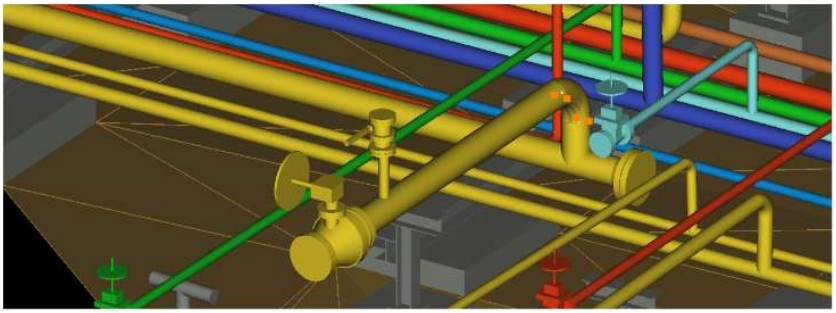

Figure 8 Elbow with surrounding objects.

3.5.3 Equipment

The equipment group consisted of two tanks and one separator. The modeling was done automatically by reconstructing the point cloud into a cylindrical surface plane. An example of the results of the tank model can be seen in Figure 9.

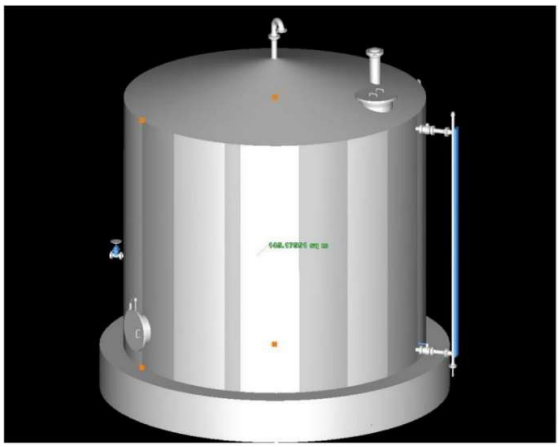

Figure 9 3D model of the tank.

3.5.4 Valve

Valve modeling was done by first breaking down the valve's point clouds into several basic structures. Each part was then modeled separately by reconstructing its basic structure into a basic geometry surface plane, e.g., cylindrical. Finally, these separate objects were merged into one complete object. Figure 10 shows an example of the point clouds of the valve and its 3D model.

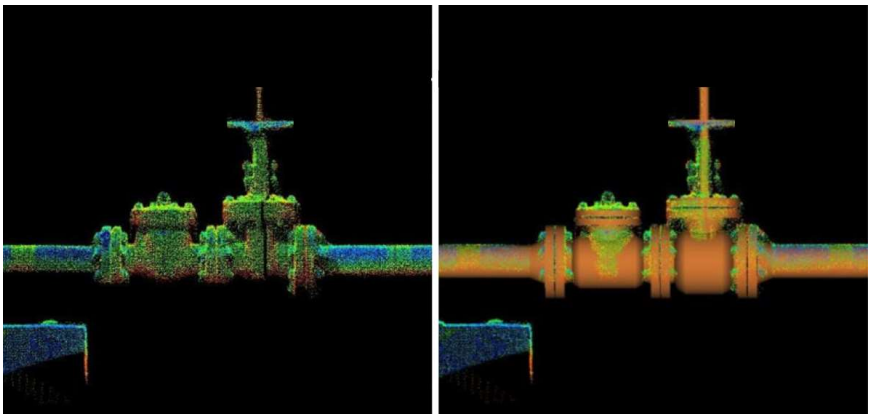

Figure 10 Point clouds of a valve (left) and its corresponding model (right).

3.5.5 Structure

On objects other than steel, structural modeling was done manually. The modeling of steel objects was done automatically by adjusting to standard sizes. Figure 11 shows an example of a structural model.

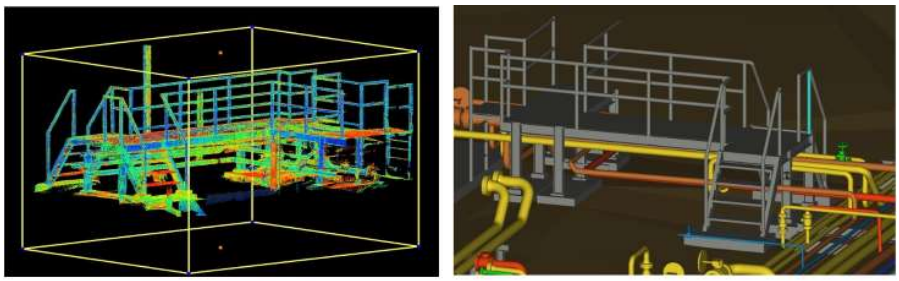

(a) (b)

Figure 11 Point clouds of structure object (a) and its corresponding model with surrounding objects (b).

3.5.6 Pipe Group

An example of a model with a pipe group according to its function can be seen in Figure 12. The colors represent the functions of the pipelines, such as gas process, liquid process, water process, drainage, diesel fuel, water instrument, water utility. The colors show the function of each pipe, e.g., cyan pipes are for air, blue pipes are for water, red pipes are for drainage, yellow pipes are for gas. An overall model of the pipe instrumentation can also be seen in Figure 12.

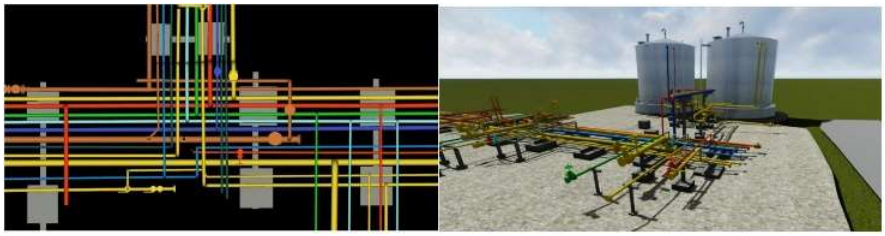

Figure 12 Initial 3D model (left) and overall 3D model (right).

3.6 Point Cloud and Model Validations

The validation process in this study was carried out by comparing the length of arbitrary samples from the global registration point clouds with the reference

values or the results of field measurements using a measuring tape. The measuring tape used had a distance measurement accuracy of 0.001 m. Some objects for validation can be seen in Figure 13. The results of the validation between the results of the point clouds and the measurement results of the reference measuring tape can be seen in Table 3.

Table 3 shows that the difference between the distance and diameter size data in the registered point cloud to the reference and field size had a largest absolute difference of 0.0034 m and an average absolute difference of 0.0016 m. These discrepancies are likely associated with the point density of the generated point clouds, causing inaccurate selection of the starting and ending points of distance measurements in the point clouds. Kankare, *et al.* [27] has reported that the accuracy of point clouds depends on point density. Nevertheless, these validation results support the claimed accuracy of the use of TLS and HS.

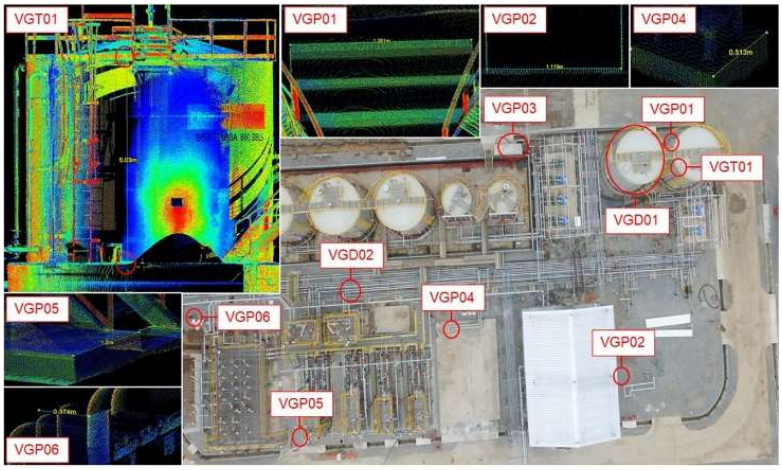

Figure 13 The objects used in the validation process.

Table 3 Geometric validation (in meters).

ID	Reference	Data	Difference
VGP01	1.2610	1.2608	0.0002
VGP02	1.1170	1.1191	-0.0021
VGP03	3.7450	3.7423	0.0027
VGP04	0.5110	0.5125	-0.0015
VGP05	1.2000	1.1997	0.0003
VGP06	0.3710	0.3744	-0.0034
VGT01	5.0300	5.0301	-0.0001
VGD01	5.8200	5.8210	-0.0010
VGD02	0.1710	0.1680	0.0030

Further assessment was done on the modeled tanks. The evaluation included the comparison of the volume and radius of the tank between the modeled and the fabrication information. The calculation of the volume was done using the Cyclone module that enables the user to estimate the volume from a generated 3D model. However, it should be noted that the calculation was made based on the outer shelf of the tank. Consequently, it does not correctly reflect the volume of the tank's capacity. The volume of the first and the second tank was calculated to be 134.11 m^3 and 134.07 m^3, respectively. The estimated volume for both tanks was slightly larger than the tank's design. The tanks were designed to hold fluid with a capacity of 133.87 m^3. The difference in volume calculation, i.e., the outer and inner volume, and the addition of a void in the upper part of the tank (see Fig. 13) are suspected of causing this discrepancy.

The calculation of tank radius was performed by estimating the tank's radius for every 10°. The average radius for each tank was used for comparison. The estimated radius for the respective tanks was estimated at 2,906.558 mm and 2,907.214 mm. On the other hand, the radius based on the fabrication information was reported as 2,910 mm, which is slightly higher than the estimates. Nevertheless, a discrepancy of about 2-3 mm is considered small.

4 Concluding Remarks

In relation to 3D modeling for complex objects and narrow data collection locations, such as piping instrumentation in the oil and gas industry, point clouds generated from TLS observations have several limitations. These include point clouds with low density as well as significant data voids, especially when dealing with complex objects. If the data is used for 3D modeling, then the created 3D model does not correctly represent the real object. The use of HS can complement the shortcomings of TLS. The obtained point cloud density will increase significantly by integrating the HS observation data. This occurs because the measurement distance is very close to the object compared to when using TLS. With a high level of density, the details of complex objects will be modeled better.

HS data can be combined with TLS data to make up for a lack of TLS data. The combination was carried out according to the rules of cloud-to-cloud registration. The internal accuracy for the registration between HS and TLS reached an average of 0.003 m. There are three aspects that must be considered during the combination process: using georeferenced data as reference, the use of the same scale factor and unit of measure, and overlapping parts between the two scan data sets.

The 3D model resulting from the combination of HS and TLS data showed good results. Based on the difference between the distance and diameter size data from

the registration results, the model that was made with reference data and the field size had a largest absolute difference of 0.0034 m (3.4 mm) and an average absolute difference of 0.0016 m (1.6 mm). Further, the resulting tank models showed good agreement with the design. The volume difference of the tanks was estimated at 0.24 m^3, which was likely to be due to the difference in volume calculation. The difference in tank radius was also estimated to be less than 3 mm. However, the geometry assessment was limited to only nine sampling points and tank models. A more robust evaluation can be made in the future in a similar study by incorporating more evaluation samples and methods, e.g., coordinate comparison. The 3D model results can also be adopted into Building Information Modeling (BIM) with the utilization of radio frequency identification (RFID), which supports more robust information management across users [28,29]. Finally, we highlight that the resulting models can be considered to be in level of detail (LoD) 3, which contains structural elements that reconstruct a complex object shape but are given in simplistic detail [30].

Acknowledgement

The authors thank the surveying division of PT ASABA for providing the instruments used in this study. The editor and three anonymous reviewers are acknowledged for providing constructive comments to improve this paper.

References

[1] Gumilar, I., Stiawan, A., Bramanto, B., Mulyadi B. & Abidin, H.Z., *Assessment on Topographic Mapping Using Total Station and Terrestrial Laser Scanner Technology (Case Study: Kiara Payung area, Sumedang)*, IOP Conf. Ser. Earth Environ. Sci., **389**, 012006, 2019.

[2] Mahasuwanchai, P., Athisakul, C., Sairuamyat, P., Tangchirapat, W., Leelataviwat, S. & Chucheepsakul, S., *An Alternative Method for Long-Term Monitoring of Thai Historic Pagodas Based on Terrestrial Laser Scanning Data: A Case Study of Wat Krachee in Ayutthaya*, Adv. Civ. Eng., **2021**,5587046, 2021.

[3] Keitaanniemi, A., Virtanen, J.P., Rönnholm, P., Kukko, A., Rantanen, T. & Vaaja, M.T., *The Combined Use of Slam Laser Scanning and TLS for the 3D Indoor Mapping*, Buildings, **11**, 386, 2021.

[4] Genechten, B.V., *Theory and Practice on Terrestrial Laser Scanning: Training Material based on Practical Applications*, Universidad Politecnica de Valencia Editorial, 2008.

[5] Kajzar, V., Kukutsch, R. & Heroldová, N., *Verifying the Possibilities of Using A 3D Laser Scanner in the Mining Underground*, Acta Geodyn. Geomater., **12**(1), pp. 51-58, 2015.

[6] Barber, D.M., Dallas, R.W.A. & Mills, J.P., *Laser Scanning for Architectural Conservation*, J. Arch. Conserv., **12**(1), pp. 35-52, 2006.

[7] Giel, B. & Issa, R.R.A., *Using Laser Scanning to Access the Accuracy of As-Built BIM*, in Computing in Civil Engineering, pp. 665-672. Jun. 2011.

[8] Cunha, R.R., Arrabal, C.T., Dantas, M.M. & Bassaneli, H.R., *Laser Scanner and Drone Photogrammetry: A Statistical Comparison Between 3-Dimensional Models and Its Impacts on Outdoor Crime Scene Registration*, Forensic Sci. Int., **330**, 111100, 2022.

[9] Gumilar, I., Abidin, H.Z., Putra, A.D. & Haerani, N., *3D Modelling of Mt. Talaga Bodas Crater (Indonesia) by using Terrestrial Laser Scanner for Volcano Hazard Mitigation*, AIP Conf. Proc., **1658**(050008), 2015.

[10] Wakisaka, E., Kanai, S. & Date, H., *Model-Based Next-Best-View Planning of Terrestrial Laser Scanner for HVAC Facility Renovation*," Comput. Aided Des. Appl., **15**(3), pp. 353-366, 2018.

[11] Gumilar, I., Gaol, S.V.L.L., Munarda, M., Bramanto, B. & Lukmanulhakim, A., *Tank Modeling and Its Condition Assessment using Terrestrial Laser Scanner*, IOP Conf. Ser. Earth Environ. Sci., **936**, 012004, 2021.

[12] Allard, P.H. & Mony, C., *Pipeline External Corrosion Analysis Using a 3D Laser Scanner*, in 18th World Conference on Non-destructive Testing, Durban, South Africa, 2013.

[13] Grobler, H.C.I. & Combrink, G., *An Evaluation of the Efficiency of Laser Scanning Technology in the Quantitative Analysis of Corrosion*, S. Afr. j. geomat., **6**(2), pp. 196-206, Sep. 2017.

[14] Wałach, D. & Kaczmarczyk, G.P., *Application of TLS Remote Sensing Data in the Analysis of the Load-Carrying Capacity of Structural Steel Elements*, Remote Sens.,**13**, 2759, 2021.

[15] Kawashima, K., Kanai, S. & Date, H., *As-Built Modeling of Piping System from Terrestrial Laser-Scanned Point Clouds Using Normal-Based Region Growing,* J. Comput. Des. Eng., **1**(1), pp. 13-26, 2014.

[16] Ameen, W., Al-Ahmari, A.M. & Mian, S.H., *Evaluation of Handheld Scanners for Automotive Applications,* Appl. Sci., **8**(217), 2018

[17] Park, H.K., Chung, J.W. & Kho, H.S., *Use of Hand-held Laser Scanning in the Assessment of Craniometry*, Forensic Sci. Int., **160**, pp. 200-206, 2006.

[18] Luetzenburg, G., Kroon, A. & Bjørk, A.A., *Evaluation of the Apple iPhone 12 Pro LiDAR for an Application in Geosciences*, Sci. Rep., **11**(1), pp. 1-9, 2021.

[19] Russhakim, N.A.S., *The Suitability of Terrestrial Laser Scanning for Building Survey and Mapping Applications*, in ISPRS Annals of the Photogrammetry, Remote Sensing and Spatial Information Sciences, **42**(2/W9), pp. 663-670, 2019.

[20] Abellán, A., Vilaplana, J.M. & Martínez, J., *Application of a Long-Range Terrestrial Laser Scanner to a Detailed Rockfall Study at Vall de Núria (Eastern Pyrenees, Spain)*, Eng. Geol., **88**, pp. 136-148, 2006.

[21] Hunter, G., Pinkerton, H., Airey, R. & Calvari, S., *The Application of a Long-Range Laser Scanner for Monitoring Volcanic Activity on Mount Etna*, J. Volcanol. Geotherm. Res., **123**, pp. 203-210, 2003.

[22] Fang, W., Huang, X., Zhang, F. & Li, D., *Intensity Correction of Terrestrial Laser Scanning Data by Estimating Laser Transmission Function*, IEEE Trans. Geosci. Remote Sens., **53**(2), pp. 942-951, 2015.

[23] Sánchez-Jiménez, D., Buchón-Moragues, F., Bravo, J.M. & Sánchez-Pérez, J.V., *Estimation of the Precision of a Structured Light System in Oil Paintings on Canvas*, Sensors (Switzerland), **19**, 4966, 2019.

[24] Patrucco, G., Rinaudo, F. & Spreafico, A., *A New Handheld Scanner for 3D Survey of Small Artifacts: The Stonex F6*, Int. Arch. Photogramm. Remote Sens. Spat. Inf. Sci., XLII-2/W15(2/W15), pp. 895-901, Aug. 2019.

[25] Hendriatiningsih, S., Suwardhi, D. & Januragadi, J., *3D Model Based on Terrestrial Laser Scanning (TLS) Case Study: The Cangkuang Temple, Garut District, West Java, Indonesia*, J. Eng. Technol. Sci., **47**(1), pp. 1-19, Feb. 2015.

[26] Suwardhi, D., Setan, H., Chong, A.K. & Rajion, Z., *Coordinate Systems Integration for Craniofacial Database from Multimodal Devices*, J. Eng. Technol. Sci., **37**(1), pp. 1-14, 2005.

[27] Kankare, V., Puttonen, E., Holopainen, M. & Hyyppä, J., *The Effect of TLS Point Cloud Sampling on Tree Detection and Diameter Measurement Accuracy,* Remote Sens. Lett., **7**(5), pp. 495-502, May 2016.

[28] Kasim, N., *Intelligent Materials Tracking System for Construction Projects Management,* J. Eng. Technol. Sci., **47**(2), pp. 218-230, 2015.

[29] Haruna, A., Shafiq, N., Ali, M.O., Mohammed, M. & Haruna, S., *Design and Construction Technique for Low Embodied Energy Building: An Analytical Network Process Approach*, J. Eng. Technol. Sci., **52**(2), pp. 166-180, Apr. 2020.

[30] Fan, H., *Automatic Derivation of Different Levels of Detail for 3D Buildings Modeled by CityGML*, Munich: International Graduate School of Science and Engineering Department of Cartography, Technische Universität München Arcisstr, 2009.